"Advanced Coatings Technologies", D. Teer and F. Rustichelli (eds.)
University of Ancona, Italy, 2002, pp. 25–44

IONIC IMPLANTATION AND CLEANING USING THE NOVEL HALL CURRENT ACCELERATOR

B. STRAUMAL[1,3], N. VERSHININ[2,3], S. POLYAKOV[3]

Abstract

Ionic sputtering and implantation technologies play an important role for the surface modification of materials. Recently, a novel Hall current accelerator has been developed. The accelerator has a large aperture of 1400 mm and a power up to 10 kW. High ionic currents up to 1 mA/cm^2 permit to use the source both for ion implantation and for ionic cleaning of substrates. Various gases can be used for both purposes: argon, nitrogen, oxygen, etc. The current-voltage characteristics for oxygen, argon and nitrogen are presented. The Hall current source advantages towards Kaufman's one in industrial processes are emphasized. The source sputter rates were measured. The maximal sputter rate is 7.5 nm/min for glass and 100 nm/min for poly(methyl metacrylate). The quality of ionic etching was demonstrated with the aid of Auger electron spectroscopy. The ionic nitriding of austenitic stainless steel and ferritic low-carbon steel has been studied. The influence of ionic current, energy of ions and implantation time are determined. The depth profiles measured with the aid of secondary-ion mass spectroscopy are presented. The hardness after ionic nitriding is characterized, the mechanism of the irradiation-enhanced nitrogen penetration in the austenitic stainless steel is discussed.

1. Introduction

Ion beam processing has become an established method for surface treatment [1]. It includes techniques like sputtering, thin film deposition or ion implantation. Though the principle is the same in all cases [2], a given application requires a

[1] I.V.T. (Institute for Vacuum Technology) Ltd., P.O. Box 47, 109180 Moscow, Russia
[2] SONG Ltd., P.O. Box 98, Chernogolovka, Moscow District, 142432 Russia
[3] Institute of Solid State Physics, Russian Academy of Sciences, Chernogolovka, Moscow District, 142432 Russia

specific source design according to the ion energy range and uniformity needed. In dependence on the energy of ions coming to the substrate, various regimes can be applied. At low energy the ions stick to the substrate and the film is formed. By increase of energy, the probability to sputter the substrate increase. The sputtering of the substrate competes with the process in the implantation of ions in the substrate. If the energy of ions is high enough, the implattation prevails. In coating technology, the substrate cleaning before coating is of particular importance for the quality of the further deposited layers, especially for their adhesion and corrosion resistance. Ion beam sputter cleaning proved to be an efficient method to produce high quality coatings on glass, metal and plastic sheets. The ionic implantation is the effective method for the surface alloying for various applications. In this paper the application of the novel Hall current accelerator both for the ionic cleaning and ionic implantation is reviewed.

2. Principle of the Hall current accelerator

For sputtering purposes, Kaufman sources [3–5] are usually chosen. These sources are very attractive in the sense that a neutralized beam is generated with the ion energy, direction and current density independently controllable. The ion production is also separated from the substrate and target used. This high degree of control and beam uniformity make Kaufman sources very competitive towards plasma processes. However, inherent design considerations limit the use of such sources in production applications [6]. The source cathode and grid optics are critical components which require sometimes an excessive maintenance. The cathode, which emits electrons to ionize the discharge gas, is subjected to erosion due to the sputtering by the ionized particles. Depending on the cathode type, the source lifetime ranges from a few hundred to one thousand of hours. Local heating or presence of active gases (such as oxygen) reduce dramatically the source lifetime by damaging the cathode. Grid optics, usually a screen grid and an accelerator grid are also subjected to erosion due to the space charge phenomenon or due to the excessive ion beam current. This somehow limits the ion beam current that can be extracted from the chamber. In glass and steel coating applications, the source design must also meet the requirement of a large area treatment. In this work, a large aperture Hall current accelerator was developed for sputter cleaning of large area glass, metal and plastic sheets. Though less controllable than Kaufman sources, a Hall current accelerator appears better suited to sputter cleaning production requirements [5]. Of greater significance is the lack of any space charge flow limitation on ion current density. Further, the reliability in etching is improved through the absence of any delicate structures like cathode or grid optics. The Hall current accelerator requires little maintenance

and sputter cleaning can be performed with active gases such as oxygen, nitrogen and carbon dioxide.

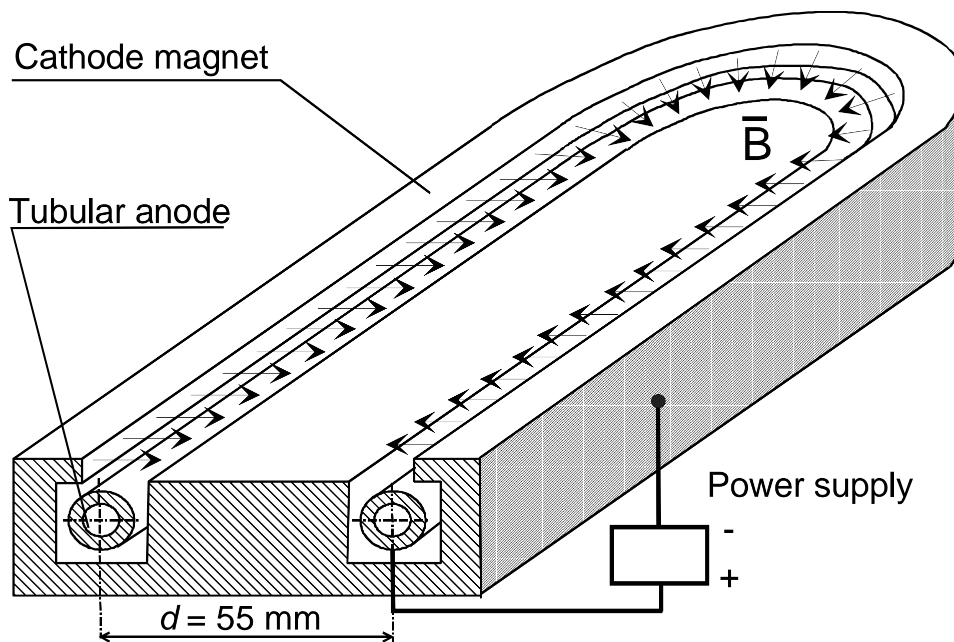

Figure 1. Hall current accelerator half view.

The Hall current accelerator is shown in Figure 1 (half view through the middle plane). It has the shape of a very elongated loop. The large aperture (1400 mm in the vertical direction) allows one to use it in the multipurpose apparatus 'Nikolay' for deposition on large area glass and plastic sheets by vacuum arc deposition and magnetron sputtering. The maximum size of the treated sheets is 2100x1300 mm. Sheets to be treated are successively transported under the Hall discharge accelerator at a given translation speed, the substrate surface being perpendicular to the ionic flux axis. Changing this speed and accelerator power, one can control the sputter dose received by the substrate. The sheet is then immediately coated to prevent recontamination. The output capacity for glass is 30 sheets in a production cycle. The source dimensions are 1400 mm in height with a twin aperture made of two slots, 55 mm away from one another. The Hall current accelerator consists of two juxtaposed permanent magnets which act as a cathode. Inside the groove made by the cathode, runs the anode of tubular shape and water cooled. The whole is set under vacuum in the presence of a sputter gas (usually argon). The gas ionization and the subsequent ion acceleration is made through the presence of crossed electric and magnetic fields. The electric field is created by the cathode to anode potential drop whereas a quasi-uniform magnetic field is set between the

two pole pieces of the cathode. In the presence of a low pressure gas and the electric field, a glow discharge plasma is initiated. The magnetic field traps the plasma electrons and together with the electric field, causes them to precess circumferentially along the anode surface. Through their cycloid path, they collide with argon atoms and ionize them. The high difference of potential accelerates argon ions away from the anode and towards the substrate to be sputter cleaned. Usual values for the source power are 6 kV and 0.5 A under an argon pressure around 0.01 Pa. The resulting ion beam has an average energy of 6 keV.

Therefore, a big progress is achieved since the early Hall current source of 10 cm aperture and ion beam energy of 50–75 eV was designed and fabricated [5]. It has been already quoted [4] that due to the unusual electron movement in Hall current accelerators, a greater energy spread, compared to Kaufman source, should be expected in the accelerated ion beam. This increased energy spread results from both charge exchange and plasma fluctuations.

3. Sputtering with the aid of Hall current accelerator

Though sputter requirements are less demanding in the production of decorative glass and steel than in microelectronics, the 'cleaning profile' of the source has to be known in order to estimate the sputter dose received by the substrates. A simple method was used to derive the source cleaning profile. 200 mm wide samples were sputter cleaned fixed to the source for different exposition times. Before cleaning, pen marks lines were drawn at a regular spacing interval on the sample surface. The pen marks provide masking against sputter cleaning of the sample surface. After cleaning treatment, they were removed with alcohol leaving a step between the sputtered and non-sputtered parts. The step height was measured using a Taylor-Hobson profilometer. The measures along the width of the sample give the cleaning distribution of the source for a given exposition time. Such experiments were carried out on silicate glass and poly(methyl metacrylate) samples. The source was also characterized with aluminum samples. Cold rolled Pechiney 5182 Al alloy was used containing 4.65 wt.% Mg, 0.37 wt.%, 0.03 wt.% Cu, 0.25 wt.% Fe, and 0.1 wt.% Si. In this study, the cleaning distribution was derived from microhardness measurements. 200×100×0.24 mm aluminum strips were sputter cleaned fixed to the source for different exposition times. Each sample was divided into ten smaller strips 20 mm wide. The initial microhardness was measured. After sputter cleaning, an average microhardness value was computed for each of the ten strips giving the profile of microhardness variation. Samples in both studies were placed 300 mm away from the source. Hence it gives conservative measures for the glass treatment as it corresponds to

the furthest glass position from the source. The current-voltage characteristic for argon at $P = 2.4\times10^{-2}$ Pa is presented in figure 2.

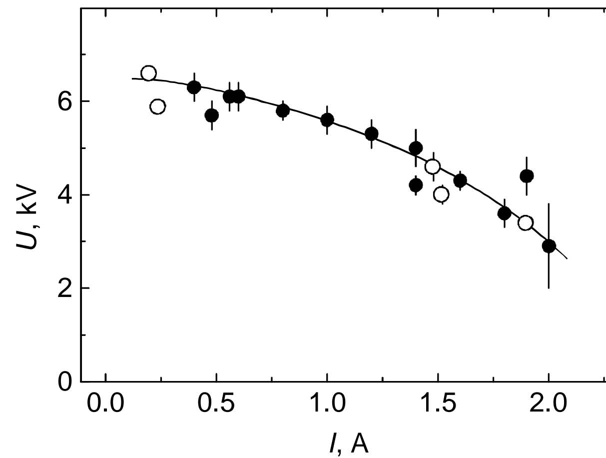

Fig. 2. Current-voltage characteristic for Ar at a pressure of 2.4×10^{-2} Pa. Gas input into the vacuum chamber (full symbols) and into the Hall accelerator (open symbols). The line is a guide for the eye.

At high voltages the current changes slowly. Below 3 kV the current starts to decrease, and the dicharge becomes unstable. The parameters of discharge are rather independent on the method of gas input (into vacuum chamber or directly into Hall accelerator). The current-voltage characteristic for oxygen at $P = 3.8\times10^{-2}$ Pa is presented in figure 3.

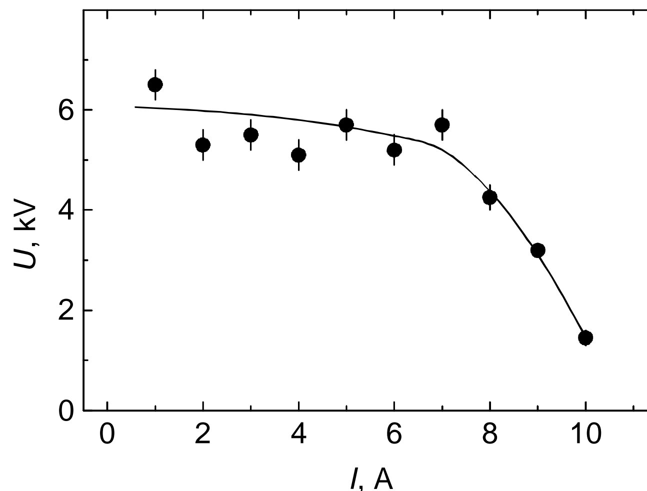

Fig. 3. Current-voltage characteristic for oxygen at a pressure of 3.8×10^{-2} Pa. The line is a guide for the eye.

The interval of stable discharge is much broader in this case (discharge current up to 6 A). The measured current-voltage characteristics allow one to optimize the regime of sputter cleaning by finding the maximum power value at a stable discharge.

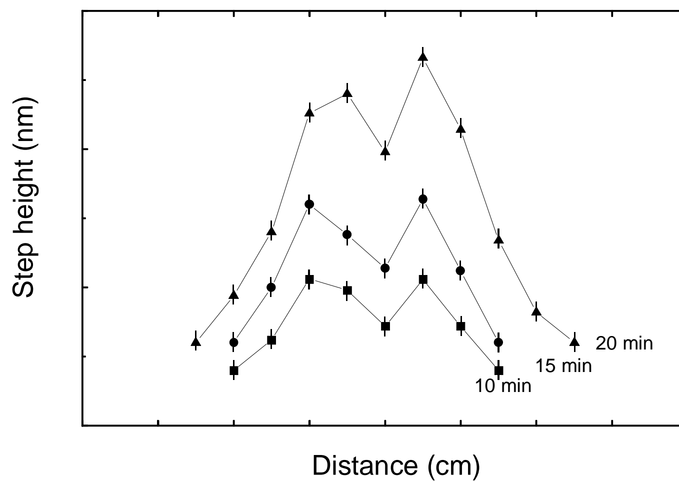

Fig. 4. Source cleaning profile for silicate glass (various sputter times)

Cleaning profiles are shown for silicate glass (figure 4) and poly(methyl metacrylate) (figure 5). As would be expected, the profile depends on the material cleaned because silicate glass and poly(methyl metacrylate) have different behaviours towards sputtering.

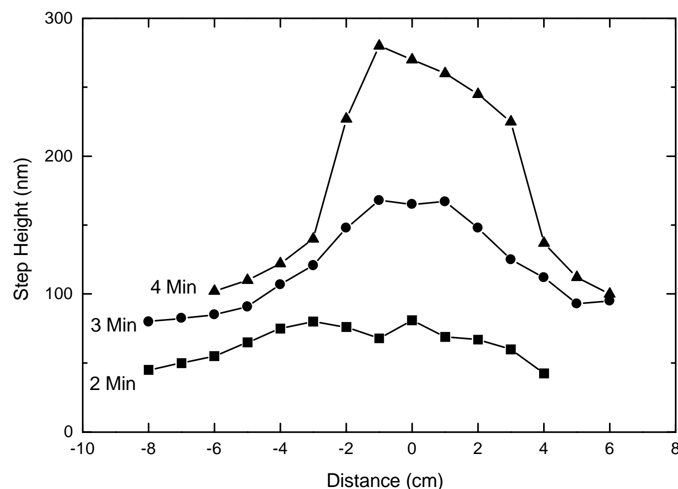

Fig. 5. Source cleaning profile for poly(methyl metacrylate).

Poly(methyl metacrylate) has a lower thermal resistance compared to silicate glass. Sputtering times beyond five minutes lead to poly(methyl metacrylate) deterioration. Below this value, the material is sputtered at a maximum rate of a 100 nm/min (Figure 5). Some reaction occurs with the sample as the surface is covered with a slightly brown layer. The cleaning distribution for organic glass is not simple as a combined physical and thermal sputtering seems to take place. As time is increased, the band of maximum sputtering is getting narrower down to around 20 mm. Silicate glass has a more reproductible cleaning profile with time (Figure 4) in comparison with poly(methyl metacrylate). The main difference is the appearance of two distinct peaks in the distribution. The twin construction of the source can hence be resolved in the cleaning profile of silicate glass. In the region of maximum sputter cleaning (corresponding to the two peaks), the sputter rate for glass is 7.5 nm/min. For silicate glass, longer times are needed to obtain significant and measurable steps. The sputter cleaning of two materials of interest showed that the source cleaning profile is highly non-uniform and material dependent. The source profile for organic glass is difficult to interpret as the ion bombardment produces a combined effect of physical and thermal sputtering on the low thermal resistance polymer. Material deterioration similar to the damage induced by ionizing radiation can be expected [7].

The source cleaning profile for glass shows a distribution in agreement with the twin aperture source design. In the first approximation, the source profile can be modelled with a two-peaks Gaussian profile distribution. 300 mm away from the source, the spacing between the Gaussian peaks (30 mm) is smaller than the distance d between the axes of elongated parts of the anode loop (Fig. 1). This shows that source beam is convergent and that a complete beam description would imply the derivation of the source cleaning profile for different distances from the source. As far as the process is concerned, silicate glass substrates, when cleaned, are moved relative to the source at a given translation speed. It ensures a uniform cleaning treatment over the glass panel surface. An estimation of the layer sputtered when moving at a given speed can be obtained by integrating the cleaning profile (expressed in cleaning rate units, e.g. nm/min) along the source width. For the speed range used in the industrial process, the silicate glass sputtered layer varies from 13 nm at low speed to 0.6 nm at high speed. At the most widely used speed, the thickness of the removed layer is 2 nm. Therefore, the Hall current accelerator can be effectively used for the sputtering of the large area glass and plastic sheets [8].

Aluminum samples observation after treatment shows a change in the surface finish at the location of maximal sputtering. This 60 to 80 mm wide area is spotted by a light reflection change, the surface being less reflective in this central part. The roughness in this area is lower than on the edges. For a eight minutes sputter treatment, the roughness falls down from 400 to 250 nm. The cleaning provides a

fine polishing of the surface. This application of sputtering is well known and has been already used for the finishing of optic glasses or the removal of scratches and surface strains after machining of metals. For reasonable times (8 and 10 minutes), a very thin sheet of aluminum looses its initial flatness and distorts itself due probably to the combined effect of substrate heating and relaxation of internal stresses by the partly removal of the superficial layer. Microhardness measurements show a maximal decrease in microhardness of about 40% (initial microhardness of the 5182 alloy is 100 HV). Increasing exposition time does not lower the microhardeness but widen the area of maximal relative change as shown in figure 6.

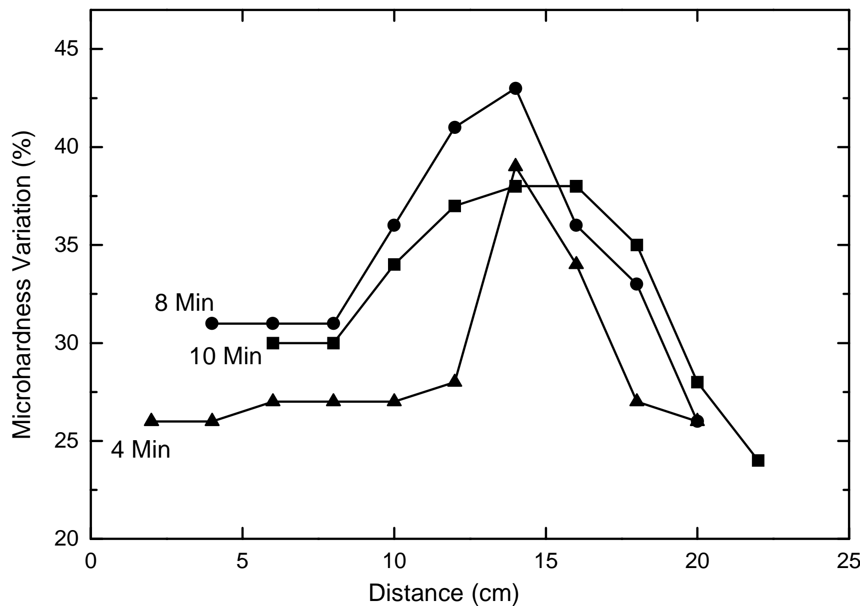

Fig. 6.
Source cleaning profile in terms of microhardness variation for Al alloy 5182.

For comparison, annealing of the 5182 aluminum alloy was done at different temperatures (200, 300 and 400°C) during 4 and 8 min. The measurements directly after treatment show a 30% decrease in the microhardness for samples annealed at 300 and 400°C. The ones annealed at 200°C did not encounter any change in the microhardness. This softening with temperature is related to the dissolution of α phase precipitates. For an Al–5 wt.% Mg alloy, the dissolution occurs at 260°C which explains that no variation was measured for the samples annealed at 200°C [9]. Cleaning of pure aluminum (99.999 wt.%) does not show any decrease in the microhardness. Annealed samples indicate that the microhardness variation is mostly due to temperature elevation. The sputtering of the superficial layer induces a little change in the overall microhardness variation.

A large aperture Hall current accelerator was presented [8]. The absence of any lifetime critical components make it very attractive for industrial applications in comparison with Kaufman sources. Little or no maintenance is needed and active gases such as oxygen and nitrogen can be used for sputter cleaning. The source sputter profile under argon was determined for silica glass and poly(methyl metacrylate) treated 300 mm away from the source. In both cases, the cleaning distribution is highly inhomogeneous and presents only a narrow area of maximal sputtering. Poly(methyl metacrylate) has a cleaning rate 13 times higher than silica glass. For this material physical sputtering is supposed to take place simultanuously with thermochemical reaction of the surface. The cleaning profile cannot be simply interpreted whereas for silica glass the two-peaks distribution induced by the twin aperture source can be resolved. Though this type of characterization does not give the full source behaviour, it enables to give an estimate of the sputtered glass layer when the substrate is moved relative to the source at a given speed. Sputter cleaning of Al alloy 5182 induces a polishing effect of the substrate surface and a 40 % decrease in the microhardness value. Increasing exposition time allows heat propagation towards the edges of the sample thus widening the area of microhardness variation without inducing a further decrease in the microhardness value.

4. Sputter cleaning with the aid of Hall current accelerator

Cleaning of aluminium has been assessed in terms of impurity content after treatment. Al 5182 samples were sputter cleaned with oxygen at a pressure of 1.5×10^{-2} Pa at different doses and immediately coated with a thin TiO_2 film less than 300 nm thick. The samples were placed in the industrial scale deposition apparatus 'Nikolay' [10]. The cleaning conditions correspond for each gas to a maximum cleaning at a low frame velocity (0.15 m/min), to medium cleaning at higher frame velocity (0.3 m/min) and no cleaning at all. The cleaning was performed through one return of the frame. The deposition parameters for the thin TiO_2 film were the same for all samples: Ti was evaporated under an oxygen pressure of 2.4×10^{-2} Pa. The samples were then analysed using Auger electron spectroscopy (AES) in order to derive the carbon content, considered as the main source of impurity. The analysis was carried out with the excitation beam normal to the specimens. The spectra were taken during argon ion sputtering which produced a relatively clean surface of the sample under study without baking the system. The etching rate was considerably faster than the adsorption rate of the active residual gases. The Auger spectra were measured on a PHI-551 spectrometer with a double-pass cylindrical mirror analyzer. The base pressure was less than 2×10^{-8} Pa. The spectra were excited by an electron beam with an energy of 3 keV and a current of 8 μA through the sample. The peak-to-peak

modulation was 3V. The sputtering was accomplished using a 5 keV Ar^+ ion beam. An ion gun was mounted to give a beam incidence angle of 70° and, in order to minimize possible crater effects, it was rastered. The pressure of argon during sputtering was equal to 3×10^{-3} Pa. In order to provide a basis for comparison, a very pure aluminium polycrystal and chemically cleaned 5182 aluminium samples were also analysed.

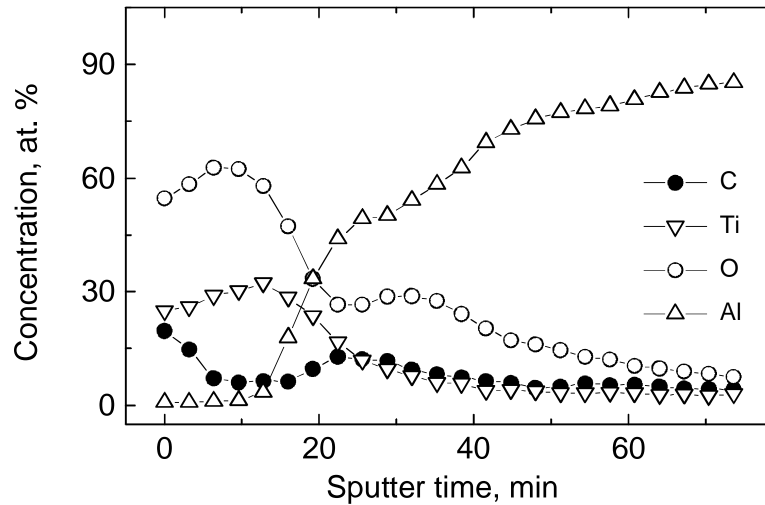

Fig. 7. AES depth profile for the 5182 Al alloy coated with TiO_2 without preliminary cleaning. The lines are guides for the eye.

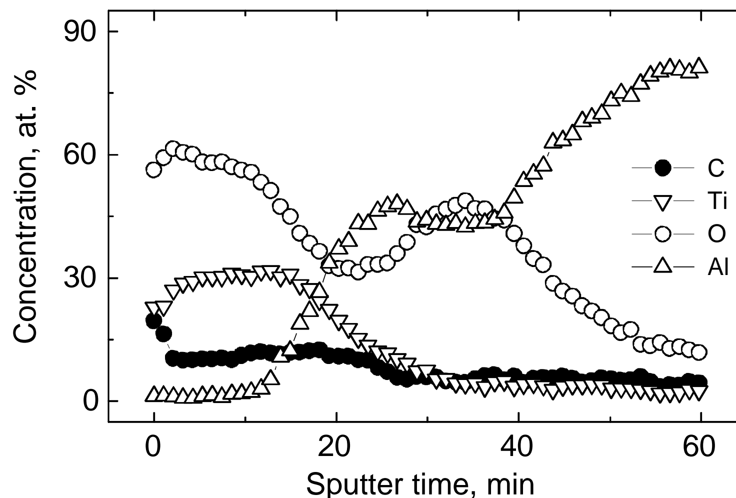

Fig. 8. AES depth profile for the 5182 Al alloy coated with TiO_2 after maximal oxygen ionic sputter cleaning. The lines are guides for the eye.

The AES depth profiles for the 5182 Al alloy without any precleaning (figure 7) and with maximal oxygen cleaning (figure 8) were measured. They show that at the surface of the samples, the carbon contamination is high and decreases deeper into the substrate. For large sputtering times, which correspond to the material bulk, the values of carbon content is still rather high (5 to 10 at. %) even for the very pure 99.999 at.% Al polycrystal. (This may be explained by the surface finish of both samples. In the experimental set up the surface sputtering is accomplished using a 5 keV Ar^+ ion beam at an incidence angle of 70°. The Auger electrons are excited by an electron beam having an other incidence than the sputtering beam. The high surface roughness may provide some shadowing making the removal of all surface contamination impossible. The oxygen content shows also a surface contamination and some implantation in the neighbourhood. In the bulk of the material, the oxygen content is equivalent to the carbon one. These preliminary spectra underline that without any treatment, the bulk of the 5182 aluminium contains around 5 at.% carbon which must be considered as the background content when reading the cleaning spectra.The spectra (figures 7 and 8) show at the beginning the presence of the thin TiO_2 film with some carbon content. The interface film/substrate is revealed by the sharp augmentation of the Al content. In this region, the carbon concentration increases in the case of the noncleaned sample while it decreases for the oxygen cleaned sample. In the bulk of the material, a 5 at.% background content is found. The second noticeable cleaning effect is observed for the oxygen content. The sputtering induces implantation close to the interface. It is revealed by a significant peak for oxygen after 30 min sputtering (figure 8). The same behaviour is observed in the case of cleaning with argon. The carbon content peak at the interface disappears when the sputtering is performed. However, no oxygen implantation occurs by sputtering with argon.

5. Ionic nitriding with the aid of Hall current accelerator

The nitriding of steels, titanium and aluminium alloys is widely used in metallurgy. In addition to the traditional methods, the ionic nitriding becomes more and more important. The ionic implantation methods traditionally used in the semiconductor technology permit to form alloyed layers buried rather deep in the material (several microns or even tens of microns) due to the high ballistic penetration depth of ions having an energy of several hundreds of keV [11]. However, this method does not fit the requirements of metallurgical applications due to the low ionic flux (below 1-3 $\mu A/cm^2$). The low intensity of ionic beams does not permit to produce metallurgically significant concentrations of an implanted element in a reasonable time. A lower energy of ions is used (20-100 keV) in the plasma immersion ionic implantation method (PIII). The lower

ballistic depth (about 100 nm) is compensated by a higher ionic flux (about 1 mA/cm^2) and additional heating of the substrate (usually to 350-400ºC) [12, 13]. PIII permits to produce the alloyed zone of 2 to 10 μm thickness. Recently the method of low-energy high-current ionic implantation (LEHCII) was developed [14, 15]. In this method the energy of ions is below 1 keV (ballistic penetration depth about 5 nm [17]) but the ionic flux is very high, reaching several mA/cm^2. Particularly, the Kaufman broad beam ionic sources are used for this purpose [12, 15]. LEHCII permits to alloy with nitrogen the surface layers of steels, having a thickness of a few μm even without additional heating [16]. Recently, a high-power large-aperture Hall current accelerator was developed [8, 17]. Hall current accelerators have several important advantages in comparison with Kaufman sources [3–6]. Particularly, the developed Hall current accelerator has a high aperture (1400 mm scalable up to 3000 mm in our case), high power (up to 10 kW), and is more robust and simple in exploitation. It is easy to combine the Hall current accelerator with existing technologies for deposition of coatings. It can be used not only for ionic cleaning [8, 17] but also for ionic implantation. Various gases can be used for both purposes: argon, nitrogen, oxygen, etc. The aim of this work is to understand the process of nitrogen penetration by low-energy high-current ionic nitriding of austenitic and ferritic steels with the aid of a Hall current accelerator.

The nitrogen implantation into austenitic stainless steel 12X18H9T and low carbon ferritic steel VSt-3-kp (Russian standard GOST 5632) was studied at discharge voltage U = 900 V, discharge current I = 3 A (ion flux density i about 1 mA/cm^2) during 30, 60 and 90 min. No additional heating of the samples was used. The composition of the steels was controlled by the spark spectral analysis according GOST 22536.13 "Carbon steel and cast iron. Methods of spectral analysis". The carbon content was measured coulombometrically according GOST 22536.1. The 12X18H9T steel contains (in wt. %) 0.11 C, 17.0 Cr, 8.8 Ni, 0.35 Ti, 0.28 Mo, 0.55 Si, 0.35 Mn, Fe (matrix). The VSt-3-kp steel contains 0.19 C, 0.12 Cr, 0.05 Si, 0.30 Mn. Samples having dimensions 20×15 mm were cut from the rolled steel strip of thickness 2 mm, ground and polished. After degreasing in ethanol and distilled water, the samples were mounted at the distance of 10 cm from the Hall current accelerator. The distribution of C, N, Fe, Cr and Ni in the samples after nitrogen ionic implantation was determined using secondary ion mass spectroscopy (SIMS). An *ims 3f* secondary ion mass spectrometer (Cameca, France) has been used for in-depth analyses of the films and substrates. O_2^+ ions accelerated with energy 12.5 kV were used as primary ions. The primary ion current I_p ranged from 250 to 1800 nA. The primary ion beam was rastered over a square area 250×250 μm. The secondary ions, accelerated by 4.5 kV, were collected from a square area 100×100 μm in the middle of the rastered area. The energy band pass filter for the secondary ions was

50 eV, centered at the maximum energy of the secondary ions. The distributions of C, N, Ti, Fe, Cr and Ni were studied by profiling isotopes $^{12}C^{-}$, $^{14}N^{-}$, $^{24}C_2^{-}$, $^{28}CO^{-}$, $^{26}CN^{-}$, $^{56}Fe^{+}$, $^{52}Cr^{+}$ and $^{60}Ni^{+}$ respectively. The $^{26}CN^{-}/^{24}C_2^{-}$ ratio was used for the estimation of nitrogen concentration by depth profiling due to the very low intensity of $^{14}N^{-}$ line. The depth of the sputtered craters was measured with a *Talysurf 10* instrument (Rank Taylor Hobson, UK). Each crater was measured several times in the central region of the crater. The deviation in the average depth ranged from 2 to 11%. The microhardness of the nitrided samples was measured at various loads (from 0.1 to 0.85 N) with the aid of *PMT* instrument (LOMO, Russia).

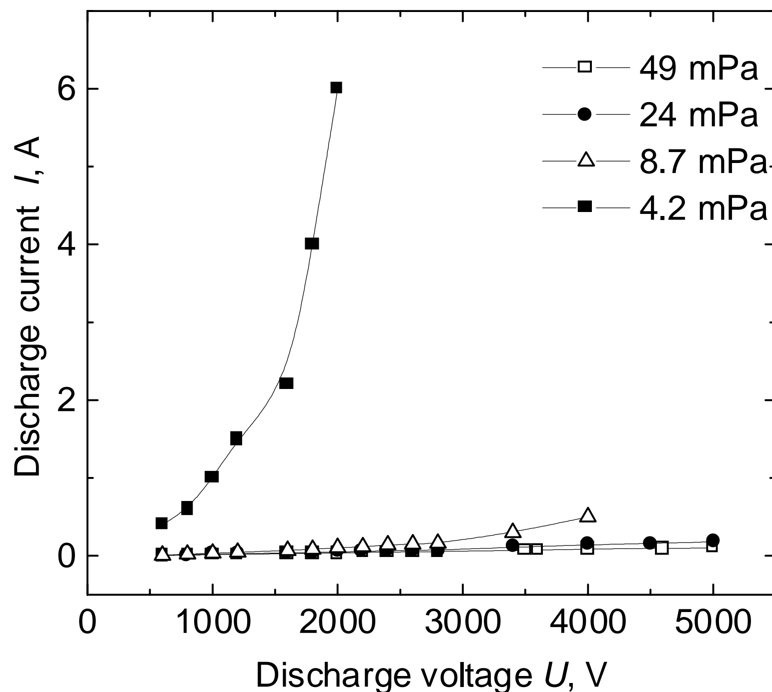

Fig. 9. Current-voltage characteristic for nitrogen at various pressures

In figure 9 the voltage-current characteristics for nitrogen discharge are shown for various nitrogen pressures *p*. It can be seen that the at *p* below 30 mPa the slow increase of discharge current *I* proceeds with increasing dicharge voltage *U*. At *p* = 49 mPa the voltage-current characteristic differs drastically from those at low *p*. The high discharge current of about 6 A can be reached already at 2 keV. In Fig. 10 the dependence of microhardness on the load is shown for the untreated stainless steel substrate and after nitriding. The indentation depth changes from 14 μm at 0.1 N (90 min) to 50 μm at 0.8 N. Therefore, at high loads the thickness of

nitrided layer is negligible in comparison with indentation depth, and the hardness of the bulk material is measured (about 3.2 GPa in all three curves). The hardness of untreated material is nearly independent of the load.

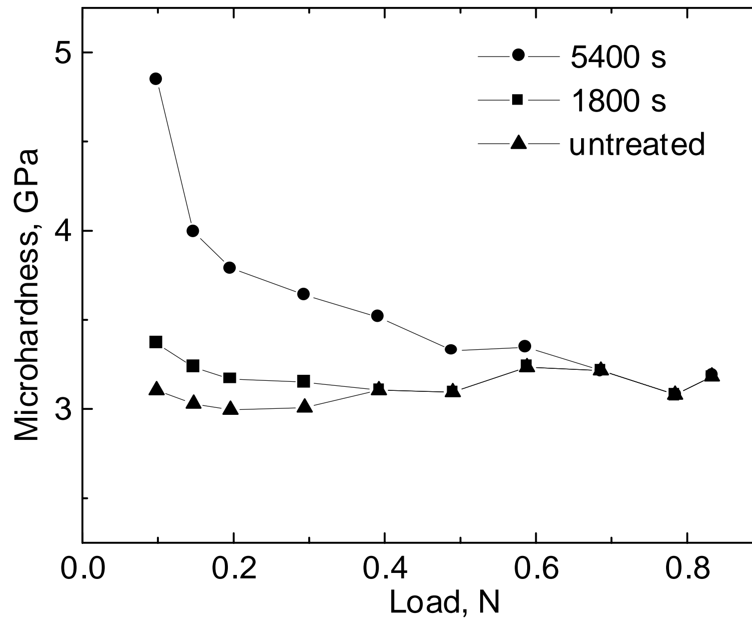

Fig. 10. Dependence of microharness on applied load for stainless steel nitrided at U = 900 V and i = 1 mA/cm^2 after various implantation times.

The implantation of nitrogen increases the surface hardness of the material. After 30 min the hardness at loads below 0.3 N is higher than that of untreated sample. With increasing duration of ionic nitriding the surface hardness increases as well. After 90 min the hardness at 0.1 N is almost two times higher than that of the untreated material. The thickness of the nitrided layer increased as well, namely the hardness drops down to the bulk value only at load of 0.6 N. The depth of the nitrided layer could be rougly estimated from the curves shown in the Fig. 9. It can be supposed that the measured hardness reaches the bulk value if the thickness of the hardened layer is less than 0.1 of indentation depth. This estimation gives about 3 µm for the thickness of the hardened layer.

In the figure 11 SIMS depth profiles are given for 30, 90 and 120 min treatments. The rough quantification of SIMS depth profiles made using the layer of Fe_4N phase on the 99.9% Fe shows that the maximal concentration of nitrogen is at least a few to 10 at. % N. The depth of nitrided layer increases with increasing implantation time t. The penetration depth for low carbon steel is slightly higher than that for stainless steel. Therefore, the estimation given above delivers overestimated values for the thickness of hardened layer. On the other hand, the microhardness

values are understimated even by load of 0.1 N. Therefore, the measurement of nanohardness with lower loads are needed for the correct estimation of the surface hardness. The thickness of the nitrided layer obtained in our experiments without additional heating of the samples is only slightly lower than that of layer obtained in comparable conditions (700 keV, 2 mA/cm^2, 60 min) by heating up to 280 °C [16].

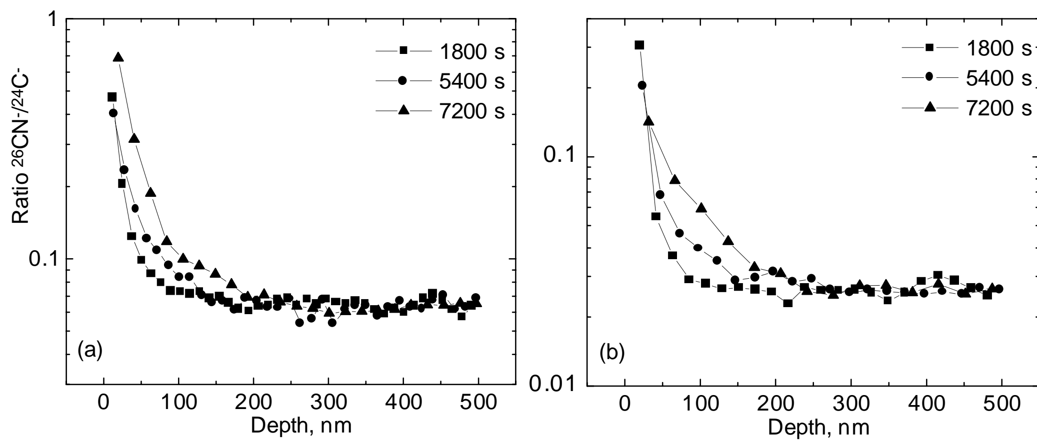

Fig. 11. SIMS depth profiles for low-carbon (a) and stainless steel (b) nitrided at U = 900 V and i = 1 mA/cm^2 after various implantation times.

The thickness of penetration layer is two orders of magnitude higher than the ballistic penetration depth for 900 V and about 2 to 4 orders of magnitude higher than the length of conventional bulk diffusion of nitrogen. Therefore, the paradoxally deep penetration of nitrogen cannot be explained neither by ballistic penetration nor by conventional diffusion. The mechanism of this process seems unusual and needs to be clarified. In particular, the role of very high ionic current and possible non-equlibrium phase transformations have to be studied. The data for the bulk diffusion coefficient (D) of nitrogen and the effective diffusion coefficient $D_{eff} = L^2/t$ (t being the implantation duration and L the penetration depth) during ion implantation are plotted in Fig. 12. The data for the bulk diffusion in α-Fe and γ-Fe are taken from the literature [18]. The extrapolation of the data for γ-Fe into α-Fe area is shown by thin line. The experimental points for bulk diffusion of nitrogen in AISI 316 austenitic stainless steel (SS) measured in the temperature range 400-500°C [19] are lower than the D data for γ-Fe extrapolated into the α-Fe area. The activation energy Q for the diffusion of N in 316 SS is only slightly higher than Q for the bulk diffusion of N in γ-Fe. The low-voltage high-current nitrogen ion implantation into AISI 304 stainless steel was studied recently [14].

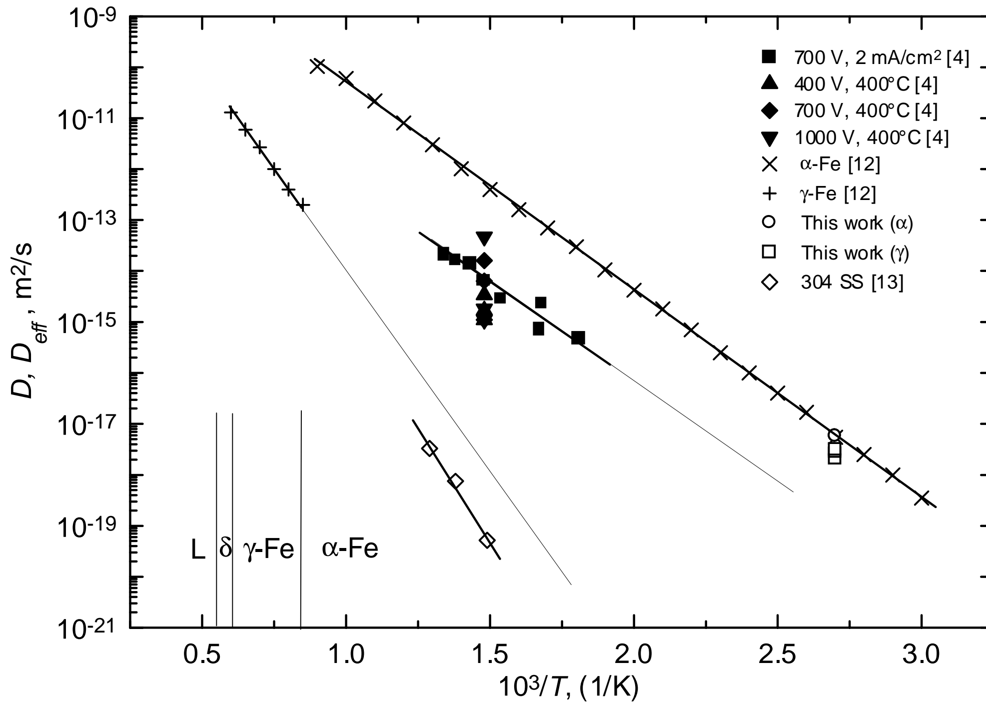

Fig. 12. The temperature dependence (Arrhenius plot) for the diffusion coefficient *D* of nitrogen in α-Fe [18], γ-Fe [18] and stainless steel [19] and for the effective diffusion coefficient estimated as $D_{eff} = L^2/t$ for the low-energy high-current ionic implantation of nitrogen. The values of D_{eff} were calculated using the data [14] for the influence of *U* and *i* at 400°C and for the temperature influence at *U* = 700 eV and *i* = 2 mA/cm^2. The data for the influence of the implantation time on D_{eff} in stainless steel (γ) and low-carbon steel (α) into non-heated substrate were obtained in this work.

It has been shown that the penetration depth increases with increasing substrate temperature *T*, ion energy *U* and ionic current density *i*. We plotted these data in figure 12 as D_{eff} for comparison with the bulk diffusion of N in Fe and stainless steel [18, 19]. The D_{eff} values obtained as the result of low-energy high-current ion implantation of N are about 3 to 5 orders of magnitude higher than the extrapolated values for the bulk diffusion in γ-Fe and about 4 to 6 orders of magnitude higher than the *D* values for diffusion of N in AISI 304 stainless steel. On the other hand, D_{eff} is about one order of magnitude lower that *D* for the diffusion of N in α-Fe. The activation energy for D_{eff} at *U* = 700 V and *i* = 2 mA/cm^2 in the temperature range 200-600°C is lower than the activation energy for the bulk diffusion of N in γ-Fe and 304 SS; it is close to the value for the diffusion of N in α-Fe. At *T* = 400°C and *i* = 2 mA/cm^2, the D_{eff} value for the ion

implantation at U = 700 V is higher than D_{eff} (U = 400 V) and lower than D_{eff} (U = 1000 V). At T = 400°C and U = 700 V, the D_{eff} value for i = 2 mA/cm^2 is higher than D_{eff} (i = 1 mA/cm^2) and lower than D_{eff} (i = 3 mA/cm^2).
The high penetration depth of N in austenitic stainless steel cannot be explained by ballistic penetration of the nitrogen ions it is only about 10 nm since for the energy studied (700-1000 eV) [16]. Due to the high density of the ion flux, low-energy ion implantation is a very non-equilibrium process. Particularly, during the nitrogen implantation into austenitic stainless steel, a layer of supersaturated solid solution is formed called *expanded austenite* with a N content exceeding the equilibrium solubility of N in γ-Fe [12]. Under certain conditions, the resulting mechanical stresses can lead to the formation of an amorphous phase in the implanted zone [20–22]. The data on the microstructural investigation of the low-energy high-current N-implanted layer in the austenitic stainless steel reveal the existence of amorphous and nanostructured layers in the implanted zone [23]. The step-like form of the penetration profiles of N after low-energy high-current implantation reveals also the existence of a surface layer with a high diffusivity [14]. The high diffusivity in the N-implanted layers can be explained by the formation of amorphous or nanograined material. Recently it was shown that grain boundaries (GBs) in two- or multicomponent systems can contain a stable layer of a GB phase which is unstable in the bulk [24, 25]. The presence of such a GB layer can lead to an enhancement of the GB mobility [26], GB segregation [25] and GB diffusivity [24]. In nanostructured materials up to 1/3 of all atoms can belong to the GB, and an increase of the diffusivity can be immence in comparison with coarce-grained materials. We can suppose that in the N-implanted stainless steel the layers of α-phase having higher diffusivity are present in GBs of the γ-matrix. Such layers can be responsible (a) for D_{eff} values which are higher than the D values for γ-Fe but lower than those for α-Fe and (b) for an activation energy Q which is close to the Q value for α-Fe.

The elevated temperature in the experiments [14] could lead to a dynamic relaxation of the defects generated during the implantation process. Therefore, in our experiments we studied the low-energy high-current N implantation without additional heating of the substrate, in order to reduce a possible dynamic relaxation of the defects. As a result, our data for D_{eff} in austenitic stainless steel are really higher than the extrapolation of the Arrhenius plot for the data taken from [14] (Fig. 12, thin solid line). The obtained D_{eff} value is very close to the D values for the bulk diffusion in α-Fe. On the other hand, the D_{eff} values obtained for ferritic (α) low-carbon steel are not much higher than those for austenictic (γ) stainless steel and practically coincide with the D values for α-Fe (Fig. 12). We investigated also the influence of the implantation duration t that was not studied

in [14] (Fig. 11). The resulting D_{eff} values reasonably coincide both for the ferritic and austenitic steels studied (Fig. 12). These facts support the hypothesis that the diffusion controls the enhanced N penetration during the low-energy high-current ion implantation into the stainless steel, and that this diffusion proceeds along the GB layers having a high diffusivity.

Acknowledgements

Authors wish to thank Prof. W. Gust, Dr. M. Benmalek, Dr. J. Bouvaist, and R. Dimitriou for fruitfull discussions. The financial support of the Copernicus network COATRANS (contract ERB IC15 CT98 0815) is heartily acknowledged.

References

1. Armour, D. G., P. Bailey, and G. Sharples. The use of ion-beams in thin-film deposition. *Vacuum, 36* (1986), 769-775.
2. Townsend P.D., J.C. Kelly, and N.E.W. Hartley. *Ion implantation, sputtering and their applications.* Academic Press, New York, 1976.
3. Kaufman, H. R. Technology of ion beam sources used in sputtering. *Adv. Electronics & Electron Phys., 36* (1974), 265-269.
4. Kaufman, H. R., J. M. E. Harper, and J. J. Cuomo. Developments in broad-beam ion source technology and application. *J. Vac. Sci. Technol., 21* (1982), 764-767.
5. Kaufman, H. R., J. J. Cuomo, and J. M. E. Harper. Technology and application of broad-beam ion sources used in sputtering. *J. Vac. Sci. Technol., 21* (1982) 725-736.
6. Kaufman, H. R. Broad-beam ion sources: Present status and future directions. *J. Vac. Sci. Technol. A, 4* (1986) 764-771.
7. Evans, D., and M.A. Crook, Irradiation of plastics: damage and gas evolution. *MRS Bulletin, 22* (1997) 36-40.
8. Vershinin, N., B. Straumal, K. Filonov, R. Dimitriou, W. Gust, and M. Benmalek. Hall current accelerator for the pre-treatment of large area glass sheets. *Thin Solid Films, 351* (1999) 190-193.
9. Massalski T. B. et al. (eds.), *Binary alloy phase diagrams*, ASM International, Materials Park, Ohio, 1990, p. 169.

10. Straumal, B., N. Vershinin, K. Filonov, R. Dimitriou, and W. Gust. Masked deposition of decorative coatings on large area glass and plastic sheets. *Thin Solid Films, 351* (1999), 204-208.

11. Bull, S.J., A.M. Jones, and A.R. McCabe. Improving the mechanical properties of steels using low energy, high temperature nitrogen ion implantation. *Surf. Coat. Technol., 83* (1996), 257-262.

12. Jiraskova, Y., C. Blawert, and O. Schneeweiss. Thermal stability of stainless steel surfaces nitrided by plasma immersion ion implantation. *Phys. Stat. Sol. (a), 175* (1999), 537-548.

13. Günzel, R., M. Betzl, I. Alphonsa, B. Ganguly, P.I. John, and S. Mukherjee. Plasma-source ion implantation compared with glow-discharge plasma nitriding of stainless steel. *Surf. Coat. Technol., 112* (1999), 307-309.

14. Williamson, D.L., J.A. Davis, P.J. Wilbur, J.J. Vajo, R. Wei, and J.N. Matossian. Relative roles of ion energy, ion flux, and sample temperature in low-energy nitrogen ion implantation of Fe-Cr-Ni stainless steel. *Nucl. Instr. Meth. B, 127-128* (1997) 930-934.

15. Parascandola, S., R. Günzel, R. Grötschel, E. Richter, and W. Möller. Analysis of deuterium induced nuclear reactions giving criteria for the formation process of expanded austenite. *Nucl. Instrum. Meth. B, 136-138* (1998), 1281-1285.

16. Pleshivzev, N.V., and A.A. Bazhin. *Physics of the Influence of Ionic Beams on Materials*. Vusovskaja Kniga Publishers, Moscow, 1998, p. 32 (in Russian).

17. Vershinin, N., R. Dimitriou, M. Benmalek, B. Straumal, W. Gust, J. Vivas, and J. Shulga. Pre-treatment of large area strips with the aid of a high power Hall current accelerator. *Surf. Coat. Techn., 125* (2000), 35-39.

18. H. Mehrer (ed.), *Diffusion in Solid Metals and Alloys*, Landolt–Börnstein New Series, Springer-Verlag, Berlin, III/26, 1990, p. 496.

19. Hirvonen, J., and A. Anttila, Annealing behaviour of implanted nitrogen in ALSI-316 stainless steel. *Appl. Phys. Lett., 46* (1985), 835-836.

20. Ischenko, T.V., S.V. Demishev, and W. Gust. Investigation of the phase formation wave in the model of solid state amorphization. *Comput. Mater. Sci., 17* (2000), 331-335.

21. Demishev, S.V., T.V. Ischenko, S.J. Blundell, and J. Singleton. Non-linear model of the solid state amorphization. *J. Phys. Cond. Mater., 9* (1997), p. 9199-9207.

22. Demishev S.V., and T.V. Ischenko. A diffusion-controlled non-linear model of the solid state amorphization. *Defect Diff. Forum, 143-147* (1997), 1535-1540.

23. Byeli, A.V., O.V. Lobodaeva, S.K. Shykh, and V.A. Kukareko. Solid-state amorphization of a tool steel by high-current-density, low-energy nitrogen ion implantation. *Nucl. Instr. Phys. B, 103* (1995), 533-536.

24. Straumal, B., E. Rabkin, W. Lojkowski, W. Gust, and L. S. Shvindlerman. Pressure influence on the grain boundary wetting phase transition in Fe–Si alloys. *Acta Mater., 45* (1997), 1931-1940.

25. Chang, L.-S., E. Rabkin, B. Straumal, P. Lejcek, S. Hofmann, and W. Gust. Temperature dependence of the grain boundary segregation of Bi in Cu polycrystals *Scripta Mater., 37* (1997), 729-.

26. Molodov, D.A., U. Czubayko, G. Gottstein, L.S. Shvindlerman, B.B. Straumal, and W. Gust. Acceleration of grain boundary motion in Al by small additions of Ga. *Phil. Mag. Lett., 72* (1995), 361-368.